Normal mode coupling observations with a rotation sensor

M.F. Nader,[1] H. Igel,[1] A.M.G. Ferreira,[2,3] D. Al-Attar,[4] J. Wassermann[1] and K.U. Schreiber[5]

[1]*Department of Earth and Environmental Sciences, Ludwig-Maximilians-University, Theresienstr. 41, D-80333 Munich, Germany.*
E-mail: nader@geophysik.uni-muenchen.de
[2]*Department of Earth Sciences, University College London, Gower Street, London, WC1E 6BT, United Kingdom*
[3]*ICIST, DECivil, Instituto Superior Técnico, Universidade de Lisboa, Av. Rovisco Pais 1, P-1049-001 Lisbon, Portugal*
[4]*Department of Earth Sciences - Bullard Laboratories, University of Cambridge, Madingley Road, Cambridge, Cambridgeshire, CB3 0EZ, United Kingdom*
[5]*Forschungseinrichtung Satellitengeodäsie, Technical University of Munich, Fundamental Station Wettzell, Sackenriederstr. 25, D-93444 Kötzting, Germany*

SUMMARY

We present observations of cross coupled spheroidal modes in the Earth's free oscillation spectrum recorded by the vertical component G-ring laser (Geodetical Station Wettzell) of the 2011 M_w 9.0 Tohoku-Oki earthquake. In an attempt to determine which are the mechanisms responsible for spheroidal energy in a vertical axes rotational spectra, we first rule out instrumental effects as well as the effect of local heterogeneity. Secondly, we carry out simulations of an ideal rotational sensor taking into account the effects of the Earth's rotation, its hydrostatic ellipticity and structural heterogeneity, which results in a good fit to the data. Simulations considering each effect separately are performed in order to evaluate the sensitivity of rotational motions to various phenomena compared to traditional translation measurements.

Key words: Surface waves and free oscillations; Rotational seismology.

1 INTRODUCTION

The study of Earth's free oscillations is a very challenging branch of seismology in terms of instrumentation stability. High quality normal mode spectra require the continuous recording of time-series during several days with very high signal-to-noise ratio in the low-frequency band (<3 mHz). Unfortunately, even though broad-band seismic networks have increased their instrumental coverage and quality, the signal-to-noise ratio of the data decreases at low frequencies. On the other hand, seismic waves are not exclusively recorded by seismometers. Different instruments, such as superconducting gravimeters (Camp 1999), laser extensometers (Park *et al.* 2008), ring lasers (Igel *et al.* 2011; Nader *et al.* 2012) and fluid tiltmeters (Ferreira & D'Oreye 2006) for example, are also sensitive to long-period ground motions. Such instruments enable alternative observations of high-quality Earth's free oscillations, potentially providing complementary information to traditional seismometer data (Park *et al.* 2005; Ferreira & D'Oreye 2006).

For the most part, normal mode studies have focused on spheroidal modes. Observations of such type of modes, for example, gave evidence of the rigidity of the Earth's inner core (Dziewonski & Gilbert 1971) or, more recently, provided constraints on its anisotropic structure (Laske & Masters 1999; Beghein & Trampert 2003; Deuss *et al.* 2010). This would not have been possible without stable, long time-series of vertical component displacements corresponding to high-quality spectra at very long

periods. Moreover, superconducting gravimeters have largely enhanced those observations (Widmer-Schnidrig 2003).

Conversely, resolving the fine structure of toroidal peaks remains at a very early stage since transverse component seismograms are significantly distorted by local tilts (Widmer-Schnidrig & Zürn 2009). One rare example of improvement of toroidal motion observations was achieved on data recorded by paired laser extensometers in Gran Sasso, Italy, which were used for the evaluation of the composite centroid moment tensor (CMT) source model of the 2004 Sumatra-Andaman earthquake (Park *et al.* 2008).

Active optical interferometers such as ring lasers can also be used to observe the Earth's free oscillations by recording seismically induced rotational ground motions around a local axis. The first observation of the Earth's toroidal normal modes with such an instrument was reported for the 2011, magnitude 9.0, Tohoku-Oki earthquake recorded on the vertical axis G-ring laser (GRL) system of the Geodetic Observatory Wettzell, Germany (Igel *et al.* 2011). In a further study, cross-coupling of modal types between 1.6 and 3.2 mHz was presented by Nader *et al.* (2012). Such observations make an interesting case of study and require an explanation.

In this paper, we attempt to determine which are the mechanisms responsible for the spheroidal energy observed in the vertical axis rotational spectra. We first rule out instrumental effects, tilt-ring laser coupling and the effect of local heterogeneity on the signal known as strain rotation coupling. Finally, we perform and analyze simulations considering the ellipticity of the figure, Coriolis coupling and 3-D structure effects separately, evaluating the sensitivity

of rotational motions to global effects with respect to traditional translation normal mode spectra.

2 OBSERVATIONS AND INSTRUMENT DESCRIPTION

With a moment magnitude of 9.0, the mega-thrust earthquake off the Pacific coast of Tohoku of 2011 March 11, far exceeded the moment magnitude expectations for the region (Stein & Okal 2011), being the strongest seismic motion that ever shook Japan in the last hundred years. The GRL operating in the Wettzell observatory (Germany) recorded the Earth's free oscillations excited by this event providing the opportunity to study in detail the low-frequency spectra generated by rotational motions.

The GRL is an active interferometer that operates based on the Sagnac effect. The instrument consists of two single-mode counter-propagating laser beams travelling inside a cavity. Because the ring laser system experiences an angular velocity in the direction of the Earth's rotation, the laser beam that propagates in this same direction travels a slightly longer distance than the one moving on the opposite way. As a consequence, the beams decouple with respect to each other shifting their phases according to the angular velocity of the apparatus. Once the two beams superimpose, the beat pattern of their relative phases is recorded (Schreiber *et al.* 2009). The relationship between the beat frequency and the rotation rate around the vector normal to the instrument plane is described by the Sagnac equation

$$f_s = \frac{4A}{\lambda P}\hat{\mathbf{n}}_\mathbf{r} \cdot \dot{\Omega}, \tag{1}$$

where f_s is the Sagnac beat frequency, $\dot{\Omega}$ is the rotation rate vector, λ is the laser wavelength and A, P and $\hat{n}_r$ correspond to the area, perimeter and unit normal vector of the ring laser, respectively.

Because of its horizontal position, the GRL is excited by rotations generated by horizontally polarized shear waves (SH type motion), which are analogous to toroidal modes in the context of the Earth's free oscillations. As eq. (1) indicates, the GRL measurements are not affected by translational motions of any type (Stedman 1997). The GRL measures the vertical angular velocity with a resolution of $\Delta\Omega = 1.2 \times 10^{-11}$rad/s/$\sqrt{\text{Hz}}$ (Schreiber *et al.* 2009).

In Fig. 1, we show the spectrum of the Tohoku-Oki earthquake calculated using a 48 hr-long time-series recorded by the GRL. The data were van Hann-tapered, high-pass filtered with corner frequency of 0.3 mHz and subsequently Fourier transformed. The output signal of the GRL has a nominal flat frequency response, therefore the data do not need to be instrument corrected.

All fundamental toroidal modes $_0T_\ell$ within the frequency range from 1.5 to 3.2 mHz are present in the spectrum in Fig. 1. Additionally, fundamental spheroidal modes $_0S_\ell$ with angular order between $9 \leq \ell \leq 17$ and $\ell = 20, 21, 22$ are clearly visible. The modes $_0S_{11}$ and $_0S_{18}$ are significantly offset from their theoretical PREM eigenfrequency as those might be influenced by nearby overtones. Because the eigenfrequencies of the coupled pair $_0T_{20} - {_0S_{19}}$ are very close, we can not affirm that the mode $_0S_{19}$ is present in the spectra.

2.1 Seismic rotations in a spherically symmetric Earth

The ground displacement associated with a given mode of vibration for unit excitation and for a spherically symmetric, non-rotating, perfectly elastic and isotropic (SNREI) earth model is given by Dahlen & Tromp (1998):

$$s_k(x) = {_n}\mathcal{D}_\ell(r\theta\phi)Y_{lm}(\theta, \phi), \tag{2}$$

where the index denotes $k = \{n, \ell, m, S \text{ or } T\}$ and the displacement operator $\mathcal{D}$ for each fixed overtone number n and angular degree ℓ is defined as:

$$\mathcal{D} = U\hat{r} + k^{-1}V\nabla_1 - k^{-1}W(\hat{r} \times \nabla_1), \tag{3}$$

where $\nabla_1 = \hat{\Theta}\partial_\Theta + (\sin\Theta)^{-1}\hat{\Phi}\partial_\Phi$ and U, V and W are radial eigenfunctions.
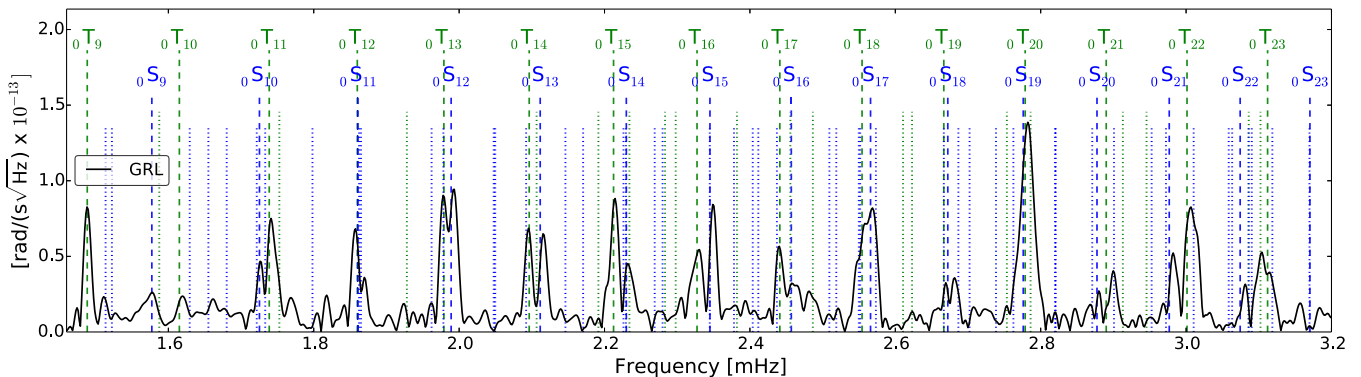
$$\mathcal{D} = U\hat{r} + \hat{\Theta}k^{-1}[V\partial_\Theta + W(\sin\Theta)^{-1}\partial_\Phi]$$
$$+ \hat{\Phi}k^{-1}[V(\sin\Theta)^{-1}\partial_\Phi - W\partial_\Theta]. \tag{4}$$

The vertical component of the rotations is obtained by taking the curl of the displacement functions (Dahlen & Tromp 1998; Ferreira & Igel 2009):

$$[\nabla \times \mathcal{D}]_{\hat{r}} = \frac{\hat{r}}{r\sin\Theta}[\partial_\Theta(\mathcal{D}_\Phi \sin\Theta) - \partial_\Phi\mathcal{D}_\Theta], \tag{5}$$

$$[\nabla \times \mathcal{D}]_{\hat{r}} = \frac{\hat{r}}{r\sin\Theta}k^{-1}[\partial_\Theta(V\partial_\Phi - W\partial_\Theta \sin\Theta)$$
$$- \partial_\Phi(V\partial_\Theta - W\sin\Theta^{-1}\partial_\Phi)]. \tag{6}$$

Because the partial derivatives in eq. (6) are interchangeable, the terms that depend on the eigenfunction V cancel out, leaving us with

Figure 1. Amplitude spectrum of 48 hr-long time-series after the M_w 9.0 Tohoku-Oki earthquake (2011) of vertical component rotations recorded at Wettzell, Germany by the G-ring laser (GRL). Dashed vertical lines indicate the non-degenerated fundamental spheroidal and toroidal eigenfrequencies while dotted lines correspond to the overtones for the earth model PREM. Fundamental toroidal and coupled spheroidal modes are clearly observed.
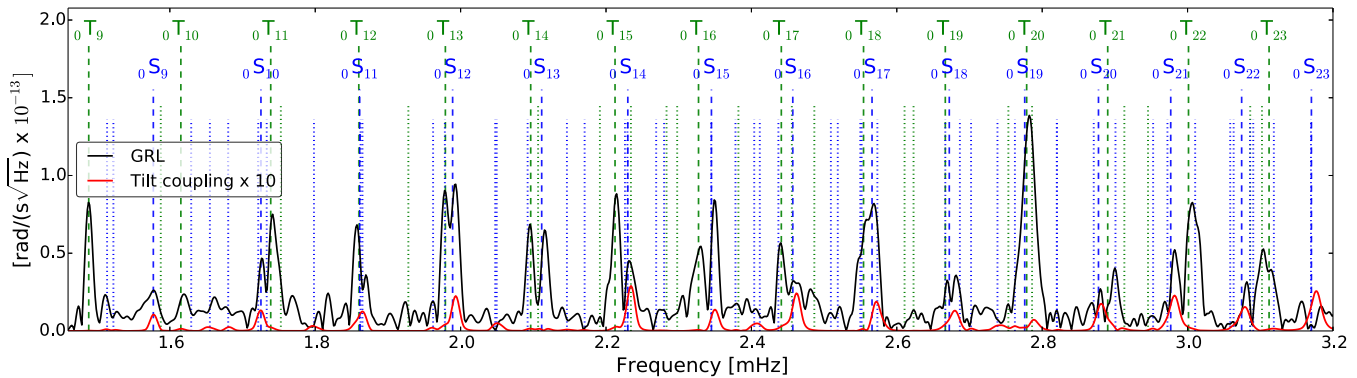
Figure 2. Same as Fig. 1 (black) and the synthetic amplitude of the tilt-ring laser coupling (red) for the 2011 Tohoku-Oki earthquake. Tilt coupling effects lead mainly to spheroidal peaks with amplitudes about 3 per cent of the observed amplitude in the vertical component rotational rate.

the expression for the vertical rotational component, which depends exclusively on the W eigenfunction:

$$[\nabla \times \mathcal{D}]_{\hat{r}} = \frac{\hat{r}}{r \sin \Theta} k^{-1} [\partial_{\Theta}^2 (-W \sin \Theta) + \partial_{\Phi}^2 (W \sin \Theta^{-1})]. \quad (7)$$

Therefore, disregarding instrumental and site effects, the vertical component of the rotational field measured by the GRL depends only on toroidal modes in a SNREI model and should be insensitive to spheroidal modes. The presence of such spheroidal modes in the spectra recorded by the GRL implies a cross coupling of motions induced by compressional waves in the vertical axis rotational spectrum. In the following section we investigate which mechanism may cause the observed spheroidal energy.

3 MECHANISMS FOR MODE COUPLING

The GRL has been the only instrument capable of recording normal mode spectra generated by seismically induced rotational ground motions. Therefore, it is necessary to estimate to what extent the specific instrumental and site conditions affect the GRL signal. We are interested in particular in the mechanisms that could couple the observed spheroidal peaks into the torsional component spectrum shown in Fig. 1. We start by considering tilt-ring laser coupling, whereby rotations around horizontal axes may affect observed vertical rotational rates. Secondly, we study strain-induced rotations due to strong local inhomogeneities. Finally, we investigate global effects such as the Earth's ellipticity, rotation and 3-D structure.

3.1 Tilt-ring laser coupling

Rotations around the horizontal axes, also known as tilts, change the orientation of the local vector normal to the instrument $\hat{n}_r$ (eq. 1). Hence, the Sagnac frequency Δf measured by the GRL will also be distorted by tilts. As a consequence, the tilt coupling causes apparent rotations which might be detected by the instrument. Tilt-ring laser coupling is generated by conversions (P-SV) and Rayleigh wave motions and consequently contributes to spheroidal frequencies in the GRL normal mode spectrum. If the tilt-ring laser coupling amplitude is significant with respect to the vertical component rotation rate, it could be the mechanism responsible for our observations.

Pham *et al.* (2009) formulated an approximate tilt-ring laser coupling expression based on the assumption that the rotational rate for active ring lasers $\dot{\Omega}$ contains both signals: the rotation rate of the Earth around its own rotation axis and the seismically induced rotation rates around vertical, north-south, and east-west axes. In

particular, the maximum tilt-ring laser coupling for a vertical axis rotational sensor is expressed as:

$$\dot{\Omega}_{\text{tilt}} = -\dot{\Omega}_P \Omega_E \cos\left(\Lambda - \frac{\Omega_E}{2}\right), \quad (8)$$

where $\dot{\Omega}_P$ is the rotation rate of the Earth, Λ is the latitude where the instrument is located and Ω_E is the east-west horizontal component of seismically induced rotations, (or coseismic tilt).

To estimate the effects of the tilt-ring laser coupling on the GRL records of the 2011 Tohoku-Oki earthquake, we calculate the corresponding Ω_E based on synthetic waveforms (see Appendix) and replace it in eq. (8). In Fig. 2 we compare the observed GRL spectrum shown in Fig. 1 with the maximum coupled amplitude. It can be seen that the maximum spheroidal amplitude due to tilt-ring laser coupling is about the 3 per cent of the total amplitudes of the vertical rotational rate recorded by the GRL. This estimation is in agreement with the tilt effects estimated by Widmer-Schnidrig & Zürn (2009) in the same frequency band for the 2002 M_w 7.9 Denali event.

Since the spheroidal peaks observed in the rotational spectrum of the GRL have similar amplitudes to the toroidal peaks, the intrinsic tilt coupling can be considered as negligible compared to the corresponding vertical rotation rate. For this reason, we are able to rule out tilt-ring laser coupling as the factor that gives rise to the spheroidal peaks in the observed spectrum.

3.2 Strain-rotation coupling

Local factors such as cavity effects (Harrison 1976), topography (Zadro & Braitenberg 1999) and geological heterogeneity (Berger & Beaumont 1976; Kohl & Levine 1995) lead to deformations of the strain field, giving rise to what is known as strain-induced rotations or strain-rotation coupling.

In a locally homogeneous and uniformly strained medium, the alignment and orientation of all the elements of the medium will be the same before, during and after straining. However, in a heterogeneous and discontinuous medium, the orientations change differently for different elements causing a local rotation of the surface. This is the reason why the measurements of a rotational sensor as the GRL will be affected by the strain-rotation coupling effect.

Strain-induced rotation is particularly important in fields that demand very stable long time-series records as tides (Lambotte *et al.* 2006) or normal mode observations (Zürn *et al.* 2000). To estimate its effect, the relation between strain and strain-induced rotation is considered linear under the conditions of linear elasticity and small

deformation. In this case, coupling constants can be defined for each location and each component, which are stable over years (Wielandt & Forbriger 1999; Lambotte *et al.* 2006).

In our specific case, the GRL measurements can be affected by horizontal strains which generate rotations around the axis normal to the surface. The horizontal strains are caused by Rayleigh wave motions. High Rayleigh wave amplitudes together with large strain-rotation coupling constants lead to spheroidal peaks in the normal mode spectrum recorded at the GRL location.

In a previous study, Driel *et al.* (2012) computed the strain-rotation coupling constants caused by the topography surrounding the Wettzell Observatory using synthetic seismograms. They also compared the simulated results with the constants estimated based on point measurements of GRL and areal rotations of a collocated array. Since the latter method is based on real data, it accounts for all possible local factors influencing such constants. The values obtained by the two different approaches were similar and considered small in comparison to other locations. Furthermore, in the same study it was shown that in order to induce a spheroidal amplitude as the observed one in the GRL spectra of Fig. 1, such constants would need to be one order of magnitude larger than what they estimated for Wettzell. Hence, strain rotation coupling can be ruled out as an explanation for the observed spheroidal peaks coupled on the GRL spectrum.

3.3 Coupling due to rotation, ellipticity and 3-D structure

The spectrum of the Earth's free oscillations can be easily calculated for a SNREI model. Deviations from that idealized model due to the ellipticity of the figure, Earth's rotation and heterogeneous structure of the Earth's interior, modify the normal mode spectrum. Coupling among mode multiplets is one of the spectral expressions of such deviations. A pair of modes couple strongly when their frequencies are close and their displacement eigenfunctions are similar. Spheroidal-toroidal mode coupling due to global effects could be the mechanism responsible for our observations. For the frequency range considered in this study, $_0S_\ell$ modes with $\ell = 6 - 25$ are closer in frequency to $_0T_{\ell+1}$ than to $_0T_{\ell-1}$, making the coupling $_0S_\ell - _0T_{\ell+1}$ the strongest.

The specific conditions in which mode coupling occurs are constrained under a set of angular selection rules established for the first time by Dahlen (1969) and lately recapitulated in Dahlen & Tromp (1998) and Widmer-Schnidrig & Laske (2007). To identify the coupling mechanism that could explain our observations, we briefly review the rules that set the conditions for the $_0S_\ell - _0T_{\ell+1}$ coupling to occur:

1. The Coriolis force acting over the wavefield results in spheroidal-toroidal coupling between modes that meet the condition $|\ell - \ell'| = 1$ for the multiplets $_nS_\ell - _{n'}T_{\ell\pm1}$. Examples of such type of coupling are the pairs $_0S_4 - _0T_3$, $_0S_{11} - _0T_{12}$ or $_1S_4 - _0T_3$.

2. The ellipticity of the Earth can give rise to spheroidal-toroidal coupling for $|\ell - \ell'| = 0$.

3. Lateral heterogeneity of harmonic degree s couples spheroidal-toroidal modes under the condition that $|\ell - \ell'| + 1 \leq s \leq \ell' + \ell - 1$ and $\ell + \ell' + s$ is odd. For example, the mode $_0S_8 - _0T_7$ is coupled through structure of degree $2 \leq s \leq 14$, where s is even.

In Fig. 3, we compare the observed amplitude spectrum at GRL (top) with a synthetic spectrum which was calculated including the effects of ellipticity, Earth's rotation and 3-D earth structure using the S20RTS (Ritsema & Van Heijst 2000) mantle model. The

forward modelling used implements full coupling in the calculations for all modes in the range 0 to 4.2 mHz (see Appendix for details on the forward modelling scheme used).

Also plotted in this figure is the same observed-synthetic spectra comparison but for the transverse acceleration (middle) and vertical acceleration (bottom) recorded at the collocated STS-2 broad-band station WET. With this, we wish to determine how accurately the synthetic spectrum of the vertical component of rotations reproduce data with respect to traditional seismometers, and to understand their differences. From the comparison, it is evident that the discrepancy between observations and modelling for the two observables is similar. To quantify the fit between synthetic and data spectra we calculate the rms amplitude misfit (eq. 9) over the 1.4 to 3.2 mHz band for both instruments, WET (vertical and transverse component) and GRL. The results are shown in Table 1.

$$\text{rms} = \sqrt{\frac{\sum_t |D(t) - S(t)|^2}{\sum_t |S(t)|^2}}. \tag{9}$$

Lentas *et al.* (2013) reported the mean spectral amplitude misfits of large magnitude (≤ 7.5) earthquakes of the past 20 yr for vertical and transverse component spectra of 0.32 and 0.48, respectively. Comparing those misfit levels with the ones obtained for the GRL and WET stations we find that data-synthetic fit of our observations falls within the typical levels.

Although the noise level in the first portion of the observed spectrum for rotations is higher than for translations, the comparison between the GRL data and synthetics makes it possible to confirm the presence of the first coupled mode pair $_0S_9 - _0T_{10}$ in the GRL spectrum. Despite a slight overestimation of the mode $_0S_9$ in the TA synthetics, the mode with larger amplitude of this pair is $_0T_{10}$ in the TA spectrum, contrary to the GRL observation, in which the amplitudes of the spheroidal and toroidal modes are similar. The second fundamental coupled pair $_0S_{10} - _0T_{11}$ is better predicted by synthetics for the rotational observable. the mode with larger amplitude of this coupled pair is opposite for the two observables as in the previous case: the T has larger amplitude in the coupled pair for rotations and the S mode for translations. Overall, the modes with larger amplitude between the coupled pairs differ between TA and GRL spectra indicating that mode coupling may be asymmetric between rotations and translations.

We can group the coupled multiplets depending on how the synthetic modes agree with data: (1) coupled modes where the fit data-synthetics is better in the rotation spectrum (e.g. $_0S_{10} - _0T_{11}$); or the opposite, that is, where TA synthetic better fit the data (e.g. $_0S_{12} - _0T_{13}$); (2) synthetic amplitude of the coupled multiplets is in good agreement with data for both observables (e.g. $_0S_{15} - _0T_{16}$); (3) the synthetic modelling over or underestimates the observed amplitudes in both spectra (e.g. $_0S_{21} - _0T_{22}$). We find examples of all these cases for both spectra.

The first observation and modelling of coupled spheroidal and toroidal modes (Masters *et al.* 1983) established the Coriolis force as the dominant mechanism responsible for the coupling between fundamental modes $_0S_\ell$ and $_0T_{\ell+1}$ in the frequency band from 1.5 to 3.0 mHz. That study focused on spheroidal-toroidal mode coupling observed in vertical component spectra. Here, we aim at identifying the main mechanism responsible for our observations of spheroidal modes in the spectra of vertical component rotations.

We perform a synthetic test comparing a reference spectrum calculated accounting for all the global effects (ellipticity, Earth's rotation and 3-D structure) with a set of spectra that include each
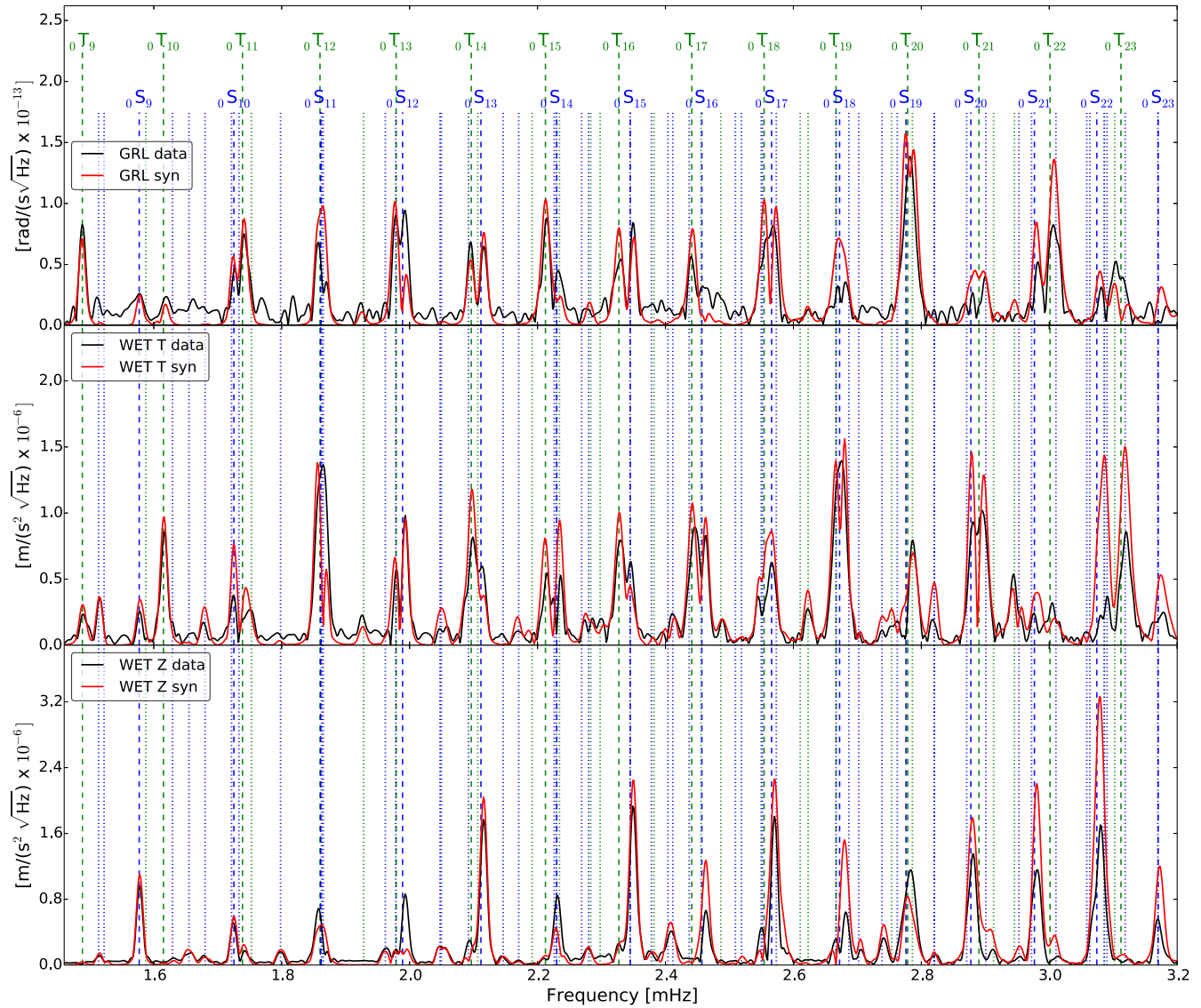
Figure 3. Comparison between synthetic (red) and observed (black) spectra of 48-hr-long vertical component rotations in GRL (top), transverse (middle), and vertical (bottom) accelerations in the WET station. The modelling includes ellipticity of the figure, rotation of the Earth and 3-D mantle model S20RTS (Ritsema & Van Heijst 2000). Dashed vertical lines indicate the fundamental spheroidal and toroidal eigenfrequencies based on PREM model (Dziewonski & Anderson 1981) while dotted lines correspond to the overtones.

Table 1. Spectral amplitude misfit values for observed-synthetic comparisons of the vertical component rotational rate recorded by the G-ring laser (GRL), the transverse (WET T) and the vertical components of acceleration (WET Z) recorded at the collocated STS-2 seismometer of the Tohoku-Oki earthquake.

| Station	rms misfit
GRL	0.44
WET T	0.45
WET Z	0.44

global effect separately. Additionally, as in Fig. 3, we compare the results for the rotational spectra with an analogous calculation but for the transverse acceleration spectra.

In Fig. 4, we show the GRL synthetic spectrum for three different simulations, each taking into account exclusively one factor:

(1) ellipticity, (2) Earth's rotation and (3) 3-D earth structure using the S20RTS mantle model.

Although most of the coupled modes $_0S_\ell - {_0}T_{\ell+1}$ within the plotted frequency interval show a small amplitude contribution to the spheroidal energy due to the effects of the 3-D mantle model, clearly the Earth's rotation through the Coriolis effect is the main mechanism responsible for the spheroidal-toroidal coupling in the vertical rotations component. In particular, the coupled pairs $_0S_{14} - {_0}T_{15}$, $_0S_{15} - {_0}T_{16}$ and $_0S_{16} - {_0}T_{17}$ are in part due to the effect of the Earth's mantle and ellipticity. Aside from the fundamental modes, there are also spheroidal overtones coupled in the GRL spectra such as $_6S_3$ (2.82 mHz) and the pair $_4S_3 - {_2}S_8$ (2.049 mHz) couple also due to the 3-D structure of the mantle.

The same analysis dissecting the effects of the different global factors was performed for the TA records (Fig. 5) to compare its behaviour with that of the vertical rotational rate observations. For the TA spectra, while many coupled modes still seem to be mainly due the Coriolis effect (e.g. $_0S_{11} - {_0}T_{12}$, $_0S_{12} - {_0}T_{13}$, $_0S_{16} - {_0}T_{17}$,
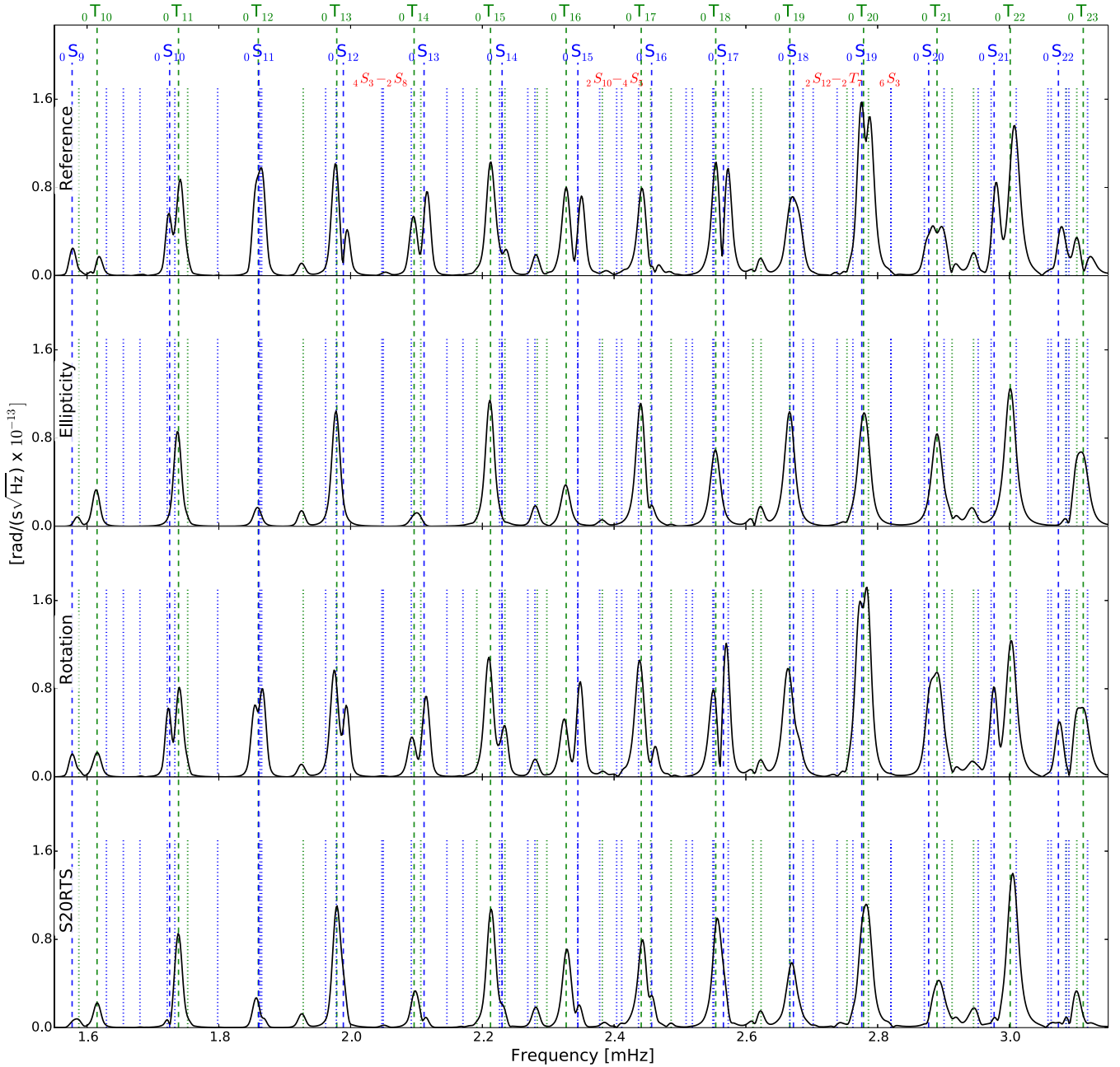
Figure 4. Synthetic spectra of 48-hr-long vertical component rotations at the GRL station. The top panel spectrum was calculated including ellipticity of the figure, rotation of the Earth and 3-D mantle model S20RTS (Ritsema & Van Heijst 2000) and is taken as a reference. In the second panel only ellipticity was used for the calculations. In the third panel only the Earth's rotation was used, and for the last one only 3-D structure. The Earth's rotation is the most effective mechanism coupling fundamental spheroidal modes in the GRL spectrum. Dashed vertical lines indicate the fundamental spheroidal and toroidal eigenfrequencies based on PREM model (Dziewonski & Anderson 1981) while dotted lines correspond to the overtones.

$_0S_{18} - {_0}T_{19}$, $_0S_{20} - {_0}T_{21}$ and $_0S_{22} - {_0}T_{23}$), ellipticity and/or 3-D earth structure also have an important contribution to some modes (e.g. $_0S_{14} - {_0}T_{15}$, $_0S_{15} - {_0}T_{16}$, $_0S_{16} - {_0}T_{17}$, $_0S_{20} - {_0}T_{21}$ and $_0S_{22} - {_0}T_{23}$) since the TA eigenfunction depend explicitly on the scalar radial function V which is associated to spheroidal motions (see eq. 7).

4 DISCUSSION AND CONCLUSIONS

We have shown that observed vertical component rotational spectra showing coupled modes is overall well fit by theoretical calculations taking into account the effects of the Earth's ellipticity, rotation and 3-D structure. Comparing the rotational spectrum with standard transverse and vertical component observations recorded at a collocated STS-2 seismometer, we find that data-synthetic misfit of the GRL is as good as the misfit levels typically found traditional seismometers in the frequency band targeted by our study. Thus, the GRL observations complements existing normal mode observations and can potentially offer a strong potential in source inversion routines of large magnitude earthquakes. We determine that $_0S_\ell - {_0}T_{\ell+1}$ coupling due to the Coriolis force associated to the Earth's rotation is the main mechanism responsible for the spheroidal modes
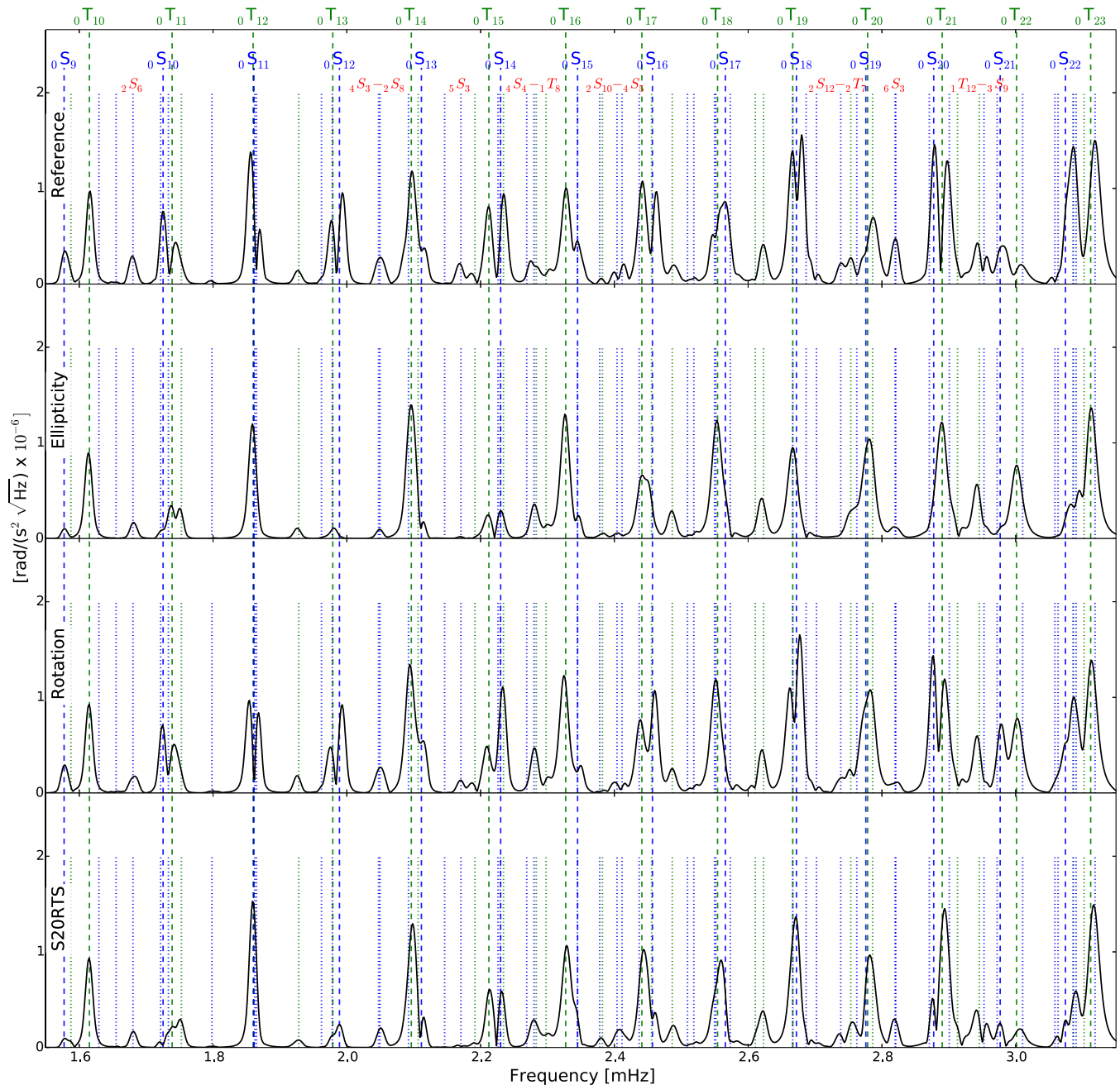
Figure 5. Same as Fig. 4 but for the transverse acceleration spectra of a collocated STS-2 seismometer.

observed in vertical component rotational spectra, ruling out instrumental and site effects. These findings are similar to previous results of studies focusing on coupled toroidal modes observed in traditional seismometer vertical component data (Masters *et al.* 1983). When analyzing seismometer transverse component data, in this study we observe that in addition to the Coriolis effect, Earth's ellipticity and 3-D structure also contribute substantially to mode coupling in the frequency range investigated. The observed differences between the coupling signature and the factors leading to mode coupling in rotations and accelerations highlight the complementarity of these two observables for normal mode studies. Because of noisy horizontal component seismometer data, there are relatively few toroidal mode measurements available (particularly for low-frequency modes), which are very important to image deep earth structure, such as seismic anisotropy (Beghein *et al.* 2008;

Hu *et al.* 2009, 2013). We expect rotational observations to help address these issues in future research.

REFERENCES

Al-Attar, D., Woodhouse, J.H. & Deuss, A., 2012. Calculation of normal mode spectra in laterally heterogeneous Earth models using an iterative direct solution method, *Geophys. J. Int.,* **189**(2), 1038–1046.

Beghein, C. & Trampert, J., 2003. Robust normal mode constraints on inner-core anisotropy from model space search, *Science,* **299**, 552–555.

Beghein, C., Resovsky, J. & Van der Hilst, R.D., 2008. The signal of mantle anisotropy in the coupling of normal modes, *Geophys. J. Int.,* **175**(3), 1209–1234.

Berger, J. & Beaumont, C., 1976. An analysis of tidal strain observations from the United States of America II. The inhomogeneous tide, *Bull. seism. Soc. Am.,* **66**(6), 1821–1846.

Camp, M.V., 1999. Measuring seismic normal modes with the GWR C021 superconducting gravimeter, *Phys. Earth planet Inter.,* **116**(14), 81–92.

Dahlen, F.A., 1969. The normal modes of a rotating, elliptical Earth-II near-resonance multiplet coupling, *Geophys. J. Int.,* **18**(4), 397–436.

Dahlen, F.A. & Tromp, J., 1998. *Theoretical Global Seismology,* Princeton Univ. Press.

Deuss, A., Irving, J.C.E. & Woodhouse, J.H., 2010. Regional variation of inner core anisotropy from seismic normal mode observations, *Science,* **328**, 1018–1020.

Driel, M., Wassermann, J., Nader, M.F., Schuberth, B.S.A. & Igel, H., 2012. Strain rotation coupling and its implications on the measurement of rotational ground motions, *J. Seism.,* **16**(4), 657–668.

Dziewonski, A.M. & Anderson, D., 1981. Preliminary reference Earth model, *Phys. Earth planet Inter.,* **25**, 297–356.

Dziewonski, A.M. & Gilbert, F., 1971. Solidity of the inner core of the earth inferred from normal mode observations, *Nature,* **234**(5330), 465–466.

Dziewonski, A.M., Chou, T.A. & Woodhouse, J.H., 1981. Determination of earthquake source parameters from waveform data for studies of global and reginal seismicity, *J. geophys. Res.* **86**, 2825–2852.

Ekström, G., Nettles, M. & Dziewonski, A.M., 2012. The global CMT project 2004–2010: centroid-moment tensors for 13,017 earthquakes, *Phys. Earth planet Inter.,* **200–201**, 1–9.

Ferreira, A.M.G. & D'Oreye, N.F., 2006. Comparison of fluid tiltmeter data with long-period seismograms: surface waves and Earth's free oscillations, *J. geophys. Res.,* **111**(B11), 307.

Ferreira, A.M.G. & Igel, H., 2009. Rotational motions of seismic surface waves in a laterally heterogeneous Earth, *Bull. seism. Soc. Am.,* **99,** 1429–1436.

Harrison, J.C., 1976. Cavity and topographic effects in tilt and strain measurement, *J. geophys. Res.,* **81**(2), 319–328.

Hu, X.G., Liu, L.T., Kroner, C. & Sun, H.P., 2009. Observation of the seismic anisotropy effects on free oscillations below 4 mHz, *J. geophys. Res.,* **114**(B7), B07301, doi:10.1029/2008JB005713.

Hu, X.-G., Hao, X.-G. & Liu, L.-T., 2013. Azimuthal anisotropy in the mantle transition zone beneath the Tibetan Plateau: evidence from normal mode coupling, *J. Geodyn.,* **64,** 54–61.

Igel, H., Nader, M.-F., Kurrle, D., Ferreira, A. M.G., Wassermann, J. & Schreiber, K.U., 2011. Observations of Earth's toroidal free oscillations with a rotation sensor: the 2011 magnitude 9.0 Tohoku-Oki earthquake, *Geophys. Res. Lett.,* **38**(21), doi:10.1029/2011GL049045.

Kohl, M. & Levine, J., 1995. Measurement and interpretation of tidal tilts in a small array, *J. geophys. Res.: Solid Earth,* **100**(94), 3929–3941.

Lambotte, S., Rivera, L. & Hinderer, J., 2006. Vertical and horizontal seismometric observations of tides, *J. Geodyn.,* **41**(1–3), 39–58.

Laske, G. & Masters, G., 1999. Limits on differential rotation of the inner core from an analysis of the Earth's free oscillations, *Nature,* **402**(6757), 66–69.

Lentas, K., Ferreira, A.M.G. & Vallée, M., 2013. Assessment of SCARDEC source parameters of global large (*M*w ≤ 7.5) subduction earthquakes, *Geophys. J. Int.,* **195**, 1989–2004.

Masters, G., Park, J. & Gilbert, F., 1983. Observations of coupled spheroidal and toroidal modes, *J. geophys. Res.: Solid Earth,* **88**(B12), 10 285–10 298.

Megies, T., Beyreuther, M., Barsch, R., Krischer, L. & Wassermann, J., 2011. ObsPy—what can it do for data centers and observatories?, *Ann. Geophys.,* **54**(1), doi:10.4401/ag-4838.

Nader, M.F., Igel, H., Ferreira, A.M.G., Kurrle, D., Wassermann, J. & Schreiber, K.U., 2012. Toroidal free oscillations of the Earth observed by a ring laser system: a comparative study, *J. Seism.,* **16**(4), 745–755.

Park, J. *et al.*, 2005. Earth's free oscillations excited by the 26 December 2004 Sumatra-Andaman earthquake, *Science,* **208,** 1139–1144.

Park, J., Amoruso, A., Crescentini, L. & Boschi, E., 2008. Long-period toroidal Earth's free oscillations from the great Sumatra-Andaman earthquake observed by paired laser extensometers in Gran Sasso, Italy, *Geophys. J. Int.,* **173**(3), 887–905.

Pham, D.N., Igel, H., Wassermann, J., Cochard, A. & Schreiber, U., 2009. The effects of tilt on interferometric rotation sensors, *Bull. seism. Soc. Am.,* **99**(2B), 1352–1365.

Ritsema, J. & Van Heijst, H.J., 2000. Seismic imaging of structural heterogeneity in Earth's mantle: evidence for large-scale mantle flow, *Sci. Prog.,* **83** (Pt 3), 243–259.

Schreiber, U., Hautmann, J., Velikoseltsev, A., Wassermann, J., Igel, H., Otero, F., Vernon, F. & Wells, P., 2009. Ring laser measurements of ground rotations for seismology, *Bull. seism. Soc. Am.,* **99,** 1190–1198.

Spudich, P. & Fletcher, J., 2009. Software for inference of dynamic ground strains and rotations and their errors from short baseline array observations of ground motions, *Bull. seism. Soc. Am.,* **99**(2B), 1480–1482.

Stedman, G.E., 1997. Ring-laser tests of fundamental physics and geophysics, *Rep. Prog. Phys.,* **60**(6), 615.

Stein, S. & Okal, E., 2011. The size of the 2011 Tohoku earthquake need not have been a surprise, *EOS, Trans. Am. geophys. Un.,* **92**(27), 227–228.

Widmer-Schnidrig, R., 2003. What can superconducting gravimeters contribute to normal-mode seismology?, *Bull. seism. Soc. Am.,* **93**(3), 1370–1380.

Widmer-Schnidrig, R. & Laske, G., 2007. Theory and observations—normal modes and surface wave measurements, in *Treatise on Geophysics,* Vol.1: Seismology and Structure of the Earth, pp. 67–125, eds Romanowicz, B. & Dziewonski, A., Elsevier Science.

Widmer-Schnidrig, R. & Zürn, W., 2009. Perspectives for ring laser gyroscopes in low-frequency seismology, *Bull. seism. Soc. Am.,* **99**(2B), 1199–1206.

Wielandt, E. & Forbriger, T., 1999. Near-field seismic displacement and tilt associated with the explosive activity of Stromboli, *Ann. Geophys.,* **42**(3), doi:10.4401/ag-3723.

Zadro, M. & Braitenberg, C., 1999. Measurements and interpretations of tilt-strain gauges in seismically active areas, *Earth-Sci. Rev.,* **47**(3–4), 151–187.

Zürn, W., Laske, G., Widmer-Schnidrig, R. & Gilbert, F., 2000. Observation of coriolis coupled modes below 1 mHz, *Geophys. J. Int.,* **143**(1), 113–118.

APPENDIX A: FORWARD MODELLING

Synthetic mode spectra were calculated using the iterative direct solution method (IDSM) in a laterally heterogeneous Earth including the effects of rotations and linear viscoelasticity (Al-Attar *et al.* 2012). This method implements full-coupling in the calculations. All modes in the range 0–4.2 mHz are included. The sampling rate for the time-series was set to 10 s and the source-time function of the event was set as a Dirac delta function. No crustal model has been included in the modelling. The mantle model used for those synthetic calculations is S20RTS with *P* velocity and density perturbations scaled to the given *S* velocity perturbation through:

$$\delta v_{\rm p}/v_{\rm p} = 0.5 \delta v_{\rm s}/v_{\rm s},$$
$$\delta \rho/\rho = 0.3 \delta v_{\rm s}/v_{\rm s}.$$

The earthquake source parameters for the forward model was taken from the Global Centroid Moment Tensor catalogue (CMT) (Dziewonski *et al.* 1981; Ekström *et al.* 2012) and is shown in Table A1.

Table A1. Global CMT catalogue parameters for the Tohoku-Oki earthquake, 2011.

CMT parameters	
Date	2011 March 11
M_W	9.0
GMT time	5:47:32.8
Lat/Lon	37.5N/143E
Depth (km)	20

Table A2. Geographical coordinates of the stations used for the synthetic calculation of vertical component rotational rate.

Station	Latitude	Longitude
Centre	49.145	12.878
North	49.2118	12.878
South	49.0782	12.878
East	49.145	12.9453
West	49.145	12.8106

A1 Filtering

To produce the time-series a cosine high-pass filter between f_{11} and f_{12} and a cosine low-pass filter between f_{21} and f_{22} have been applied where these frequencies are given by:

$f_{11} = 0.01 \, \text{mHz}$

$f_{22} = 4.0 \, \text{mHz}$

$f_{12} = f_{11} + 0.01 * (f_{22} - f_{11})$

$f_{21} = f_{22} - 0.01 * (f_{22} - f_{11}).$

A2 Rotational waveform calculation

We obtain the synthetic waveforms for the vertical component of rotations by calculating the curl in spherical coordinates. To do so, we place a station array around the GRL station with the geographical coordinates shown in Table A2 and perform a finite differentiation in spherical coordinates of the velocity seismograms between the stations. The calculation of ground strains and tilts was done with an array derived rotation method presented by Spudich & Fletcher (2009).